SPOT DEM Analysis for fault segment mapping in the Lokris region, Central Greece

Athanassios Ganas[1], Kevin White[1] and Geoff Wadge[2]

[1]Department of Geography
University of Reading, Whiteknights
Reading, RG6 6AB, UK

Tel : +44-1189-318733, Fax : +44-1189-755865

[2]Environmental Systems Science Centre
Harry Pitt Building
3 Earley Gate, Whiteknights
PO Box 238, The University of Reading, Reading RG6 6AL, UK

ABSTRACT

It is shown that SPOT 1A DEMs can be used in mapping fault segmentation patterns inside juvenile rift systems where footwall topography variations are linked to long-term fault growth rates. A remote sensing methodology is proposed involving image processing and GIS software systems. 100-m DEMs provide adequate resolution to visualise shapes of mountain ranges, extract footwall drainage patterns and measure the spatial variation of surface slope. The persistence of unimodal slope histograms over extended footwall areas (9-10 km^2), indicating similar rates of landscape evolution, may be attributed to a spatially continuous kinematic property, the footwall uplift rate. This methodology has been applied in the Lokris region (Central Greece) where both the position and length (ci. 35 km) of two active fault segments (Kammena Vourla and Kallidromon) were extracted. This information can be used as a deterministic input into seismic hazard models for the area and to calculate maximum earthquake size.

1. INTRODUCTION

Digital Elevation Models (DEMs) are regularly spaced elevation data usually digitised from cartographic sources, that have found widespread applications in the Earth Sciences. In particular, the use of these DEMs in structural mapping has been primarily into extracting lineament attributes (e.g., Murphy, 1993, Deffontaines *et al.*, 1994), mainly length and orientation. Recently, new uses of DEMs include their integration into projects mapping long-term continental and short-term earthquake deformation at regional scales (e.g., Jones *et al.*, 1996; Abbott *et al.*, 1997; Massonnet and Feigl, 1995). Moreover, SPOT-derived DEMs have been shown to match the quality of the digitised counterparts (e.g., Day and Muller, 1989; Bolstad and Stowe, 1994), and this has offered the capability of extracting raster maps of surface topography of rift systems quickly, and at high spatial resolutions (30-100 m).

This paper proposes a new use of DEMs in hazard-related mapping work. It is suggested that elevation and slope data extracted from stereopairs of satellite images, can be used to infer active fault positions in continental rift systems because inside these areas the configuration of relief may be linked with systematic variations of fault displacement (Anders and Schlische, 1994). For example, in Central Greece (Roberts and Jackson, 1991; Roberts and Koukouvelas, 1996) as well as within the Basin and Range extensional province in southwestern USA (Stein *et al.*, 1988) the surface topography is controlled by long-term growth of normal faults, which rupture in large (M>5.8) earthquakes. A simple cross-examination of 1 : 100 000 scale topographic and geologic maps of these areas indicates that the footwalls of normal faults are marked by high mountains (1-3 kilometres high), where pre-rift rocks are exposed and the elevations of these mountains change along strike. This paper shows that areas of low topography possibly marking the ends of segments can be recognised from space by the construction of DEMs of rift systems, and such elevation data can be further analysed to extract the spatial variation of morphometric parameters of relief, in order to establish the extent of footwall areas of active faults. It is suggested that this information can be used as an independent criterion to map fault segmentation patterns in rift systems. f we then make the assumption that most of seismic strain is released by slip along these major fault segments, the size (length, area) of the seismogenic sources may be extracted. In turn, this important parameter can be used in seismic hazard modelling studies or in empirical seismological relationships (e.g. Wells and Coppersmith, 1994) to calculate fault-specific surface magnitudes.

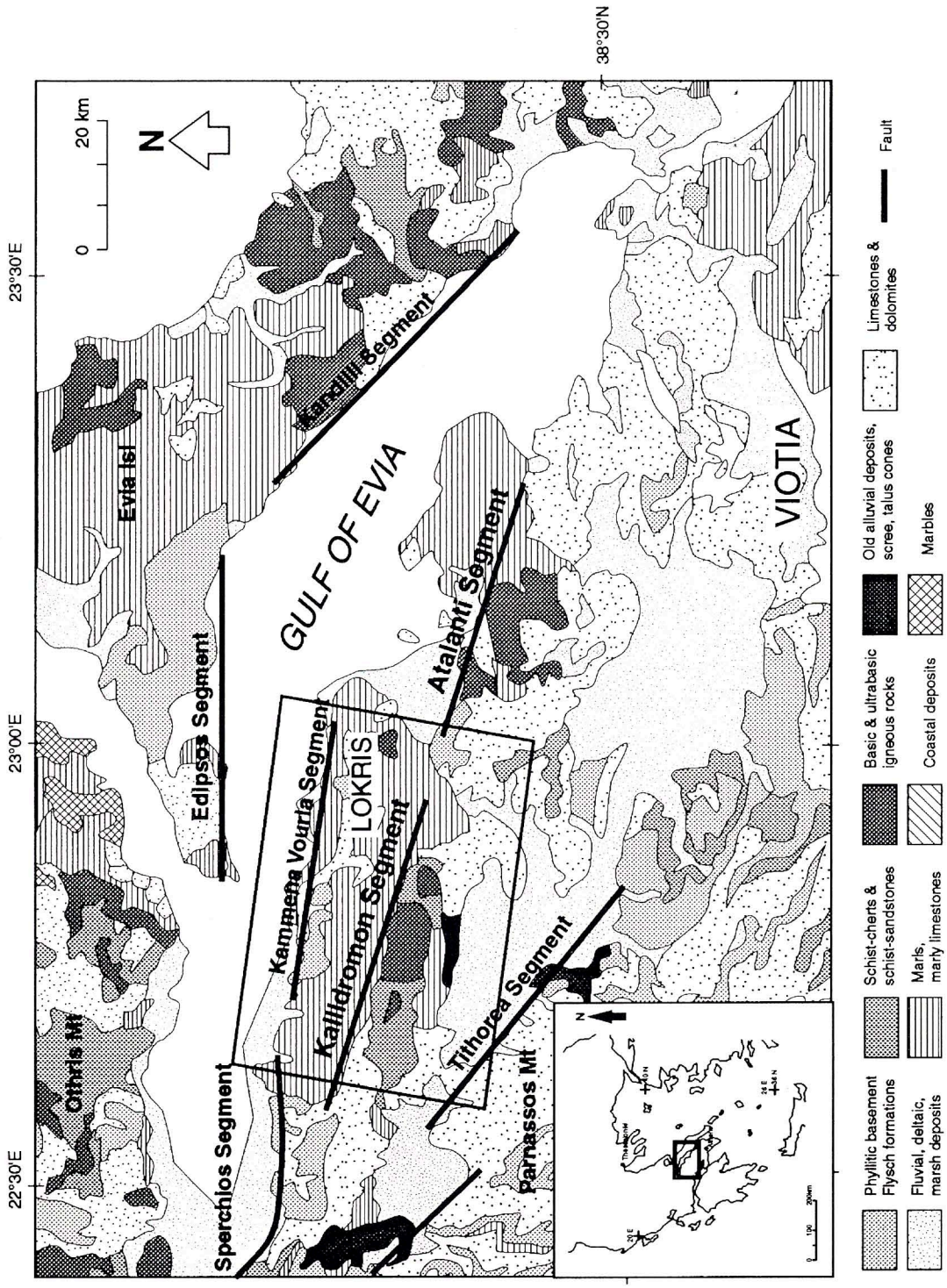

Figure 1. Geological map of Eastern Central Greece showing also positions of normal fault segments. Segment positions have been identified in Ganas and White, (1996) Ganas et al., (1996) and Ganas et al., in press. The Gulf of Evia is a 80 km WNW-ESE marine basin formed as a result of Late Quaternary crustal extension. Inclined box shows boundaries of Figure 3.

Central Greece (Figure 1), is a well known extensional province (Roberts and Jackson, 1991) where upper-crustal extension is accommodated by slip along large normal fault segments of planar geometry. This rift area has experienced large earthquakes in the historical past (Ambraseys and Jackson, 1990) and fault segmentation theory has been applied (Roberts and Jackson, 1991; Roberts and Koukouvelas, 1996; Ganas et al., in press). Using DEM analysis we present information on the length and seismogenic potential of two fault segments inside the Gulf of Evia rift, namely the Kammena Vourla and Kallidromon segments (Figure 1) located at Western Lokris.

DESCRIPTION OF METHODOLOGY

SPOT Data Characteristics

SPOT DEMS are constructed from stereomatching of level 1A products (i.e. Day and Muller, 1989). In this study a SPOT1 stereopair was used where the western half of the Gulf of Evia region is covered (scene 89/272-B/H=0.75). Both images (Table 1) were collected during January 1989 (18 days apart) and show excellent radiometric fidelity, which enhances the stereomatcher results. Moreover, they are cloud free and do not show any noticeable atmospheric effects, nor any form of pushbroom striping. However, they do suffer from E-W, relief-induced shadowing at two areas (Kammena Vourla, Zeli) and from local snow coverage at high altitudes. The shadowing problem is expected to influence stereomatcher output and consequently interpolation results may show a greatest RMS error at these areas. However, this is still tolerable in our methodology because it is the sun-facing footwall areas (which occupy most of the images and where drainage is developed) and not the hangingwall (shadow) areas that are of primary concern.

Step One : Data Processing using the 3D-Image Maker Software

The public domain software *3D-Image Maker* by the University College London (©UCL, 1990) was used to construct a 100-m DEM. A number of programs on a network of Sun workstations were utilised. The basics of the procedure followed to generate the DEM are the following :

a) Manual selection of 9 seedpoints on both SPOT images for use in the stereomatching, using the program Gview.

b) Application of the stereomatcher-program Gotcha,, which is based on the Gruen-Otto-Chau algorithm (Otto and Chau, 1989).

c) Selection of 12 ground control points from the 1:50 000 Greek topographic maps using ARC.

d) application of the camera model with reference to the ground control points, using the program Spot1.

e) Application of the Kriging interpolation method, using the program Krige_some. A linear Kriging estimator was used of the type $Z = w_1 z_1 + w_2 z_2 + \ldots + w_n z_n$, where w_i sums to 1 and z_i are the sample (elevation) values.

f) Visualisation of the results to view footwall topography using the program Evileye. g) Produce a 16-bit Sun raster file to import to other software programs for quantitative analysis, using the program Hipras.

The vertical accuracy of the DEM (z-RMSe 16.21 m) was evaluated against 56 independent spot heights (± 1m) from the National Triangulation Network of the Greek Military Geographical Service (HAGS). The horizontal accuracy was not determined, because only the relative positions of objects in the x-y plane were of interest in this study. It is suggested that a vertical standard accuracy of 16 metres is adequate for our regional study, where average elevation over the region examined is 300 metres (HAGS, 1977) and maximum elevations of mountain ranges reach 1700 metres (i.e. average z-error between 1-5% of topography). However, it is important to investigate the sources of this error for any future work. The biggest contribution to the error was the coordinate differences due to map datum shifts. In spot_1 the stereomatched points were projected to the Earth's surface using the WGS84 datum, whereas the GCPs used to calibrate the model had been collected from the 1971 Greek maps which use the European 1950 datum (Mallis, pers. comm., 1995). Other contributors to the z-error may be the error in the elevation of the GCPs which is ± 5 m (nominal) and the lack of adequate GCPs both along the coastline and in the high altitudes.

TABLE 1. DETAILS OF THE GULF OF EVIA JAN 1989 STEREOPAIR.

Characteristic	LEFT IMAGE	RIGHT IMAGE
Scene (Path/row)	089/272	089/272
Acquisition date	89/01/01 09:40:48	89/01/18 09:13:47
Orbit number	113	354
Sensor	SPOT1 HRV1 mode P	SPOT1 HRV2 mode P
Satellite Altitude (m)	830769.8	830082.3
Centre co-ordinates	N384857/E0223901	N384856/E0225709
Incidence Angle	22.32°	-18.88°
Sun azimuth (at centre pixel 3000,3000)	166.7	157.7
Sun angle(at centre pixel 3000,3000)	+27.1	+27.5
Image Orientation (clockwise North)	13.6°	9.2°

data ©UCL

Step Two : Analysis and Interpretation of DEM Data

The methodology we suggest involves three stages of computer processing: data visualisation, production of thematic elevation maps and production of slope maps. Firstly, a visualisation of the DEM in 3D image space is necessary to view the general relief configuration of the study area, in order to establish the size and orientation of the mountain ranges. A panoramic view of the produced elevation dataset (to the south) is shown in Figure 2a and a largely corresponding field photograph of the "ground truth" is shown in Figure 2b. A number of structural and geomorphic features can be seen (Figure 2a; compare with Figure 1) : The coastal Kammena Vourla Fault Segment shows the characteristic dome-shape footwall profile along its strike, as expected from isolated segmentation models (e.g., Anders and Schliesce, 1994). However, the second segment to the south, the Kallidromon Fault Segment (Figure 1) does not show this systematic variation in footwall topography but an increase in footwall elevation towards the northwest (see also Figure 3 below). It is suggested that this asymmetry may be due to the uplift of the northern part of the range by a younger normal fault segment to the north (the Sperchios Fault Segment; see Figure 1).

Secondly, the DEM was imported to *ARC-GRID* to classify elevations into 100-m classes and map drainage patterns. This is because a quick overview of elevation distribution is obtained and because of the poor DEM quality in the high-relief (shadow) areas (Figure 2a) the application of automatic drainage extraction algorithms is not possible. Drainage patterns may provide information on segment boundaries (Roberts and Jackson, 1991) and by making use of data classification techniques within the GIS a thematic elevation map can be produced so that (i) the catchment boundaries can be better delineated in order to map catchment size, distribution and obtain areal statistics and (ii) length and geometry of mountain ranges (identified by hillshading techniques) is accurately determined. Figure 3 shows a GRID image of relief in Western Lokris, from which the following interpretations can be made :

- three E-W mountain ranges can be distinguished, on the basis of the linear geometry of the height contours above 300 m.
- The mountain ranges form a characteristic "basin-and-range" structure, spaced at 10 km and their crestlines increase in height towards the south, i.e. away from the rift axis (compare with Figure 2b).
- N-S trellis drainage has developed inside the Kallidromon half-graben (area 2 in Figure 2a) except for two important E-W drainage channels that have formed with anti-diametric flows. It is suggested that these channels (diverging black arrows in Figure 3) have developed as a result of regional footwall uplift of the younger, coastal Kammena Vourla fault segment.
- In addition, it is suggested that the low relief area in the southeast part of Figure 3, where an important hydrological divide occurs for more than 5 km (Figure 3, single thin black arrow), forms a segment boundary between the Kallidromon and Atalanti Fault segments (Figure 1).

Thirdly, the DEM data were processed in ERDAS Imagine to extract a slope map. The surface slope is calculated as the change in elevation over a DEM pixel, in this case over 100 metres. A 3 × 3 pixel window is used to calculate the slope at each pixel. The slope calculation formula is $s = \frac{\sqrt{(\Delta_{EW})^2 + (\Delta_{NS})^2}}{2}$,

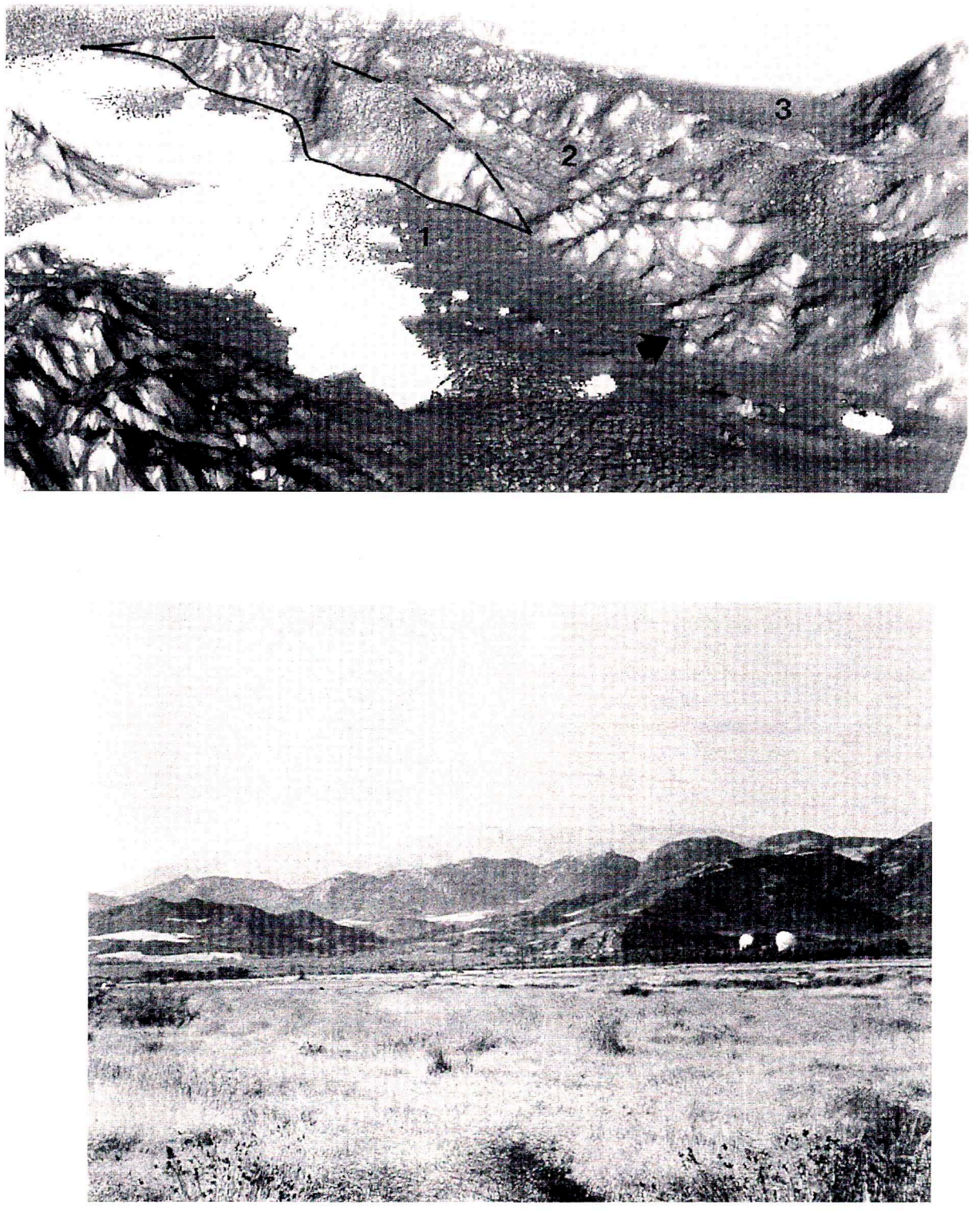

Figure 2. a) Image showing an Evileye™ program output of the western Lokris area, Central Greece. The view is towards the south and illumination is from the northwest. The Gulf of Evia is at the foreground (white). The black sinuous line indicates the trace of the Kammena Vourla Fault Segment, while the semi-elliptical dashed line highlights the domal shape of the coastal mountain range. Note that scale is not uniform because of perspective viewing geometry, and a vertical exaggeration of 5%. Numbers refer to half-graben positions with respect to the rift axis. Black arrow point to the viewing direction of Figure 2b.

b). Field photograph of normal fault segments on the south side of the Gulf of Evia Rift, Central Greece. The photograph was taken at sea level looking south. The low hill region in the foreground is the segment boundary between the Kammena Vourla and Sperchios Fault Segments (see Figure 1). Also shown in the background are the Kallidromon and Tithorea Fault Segments.

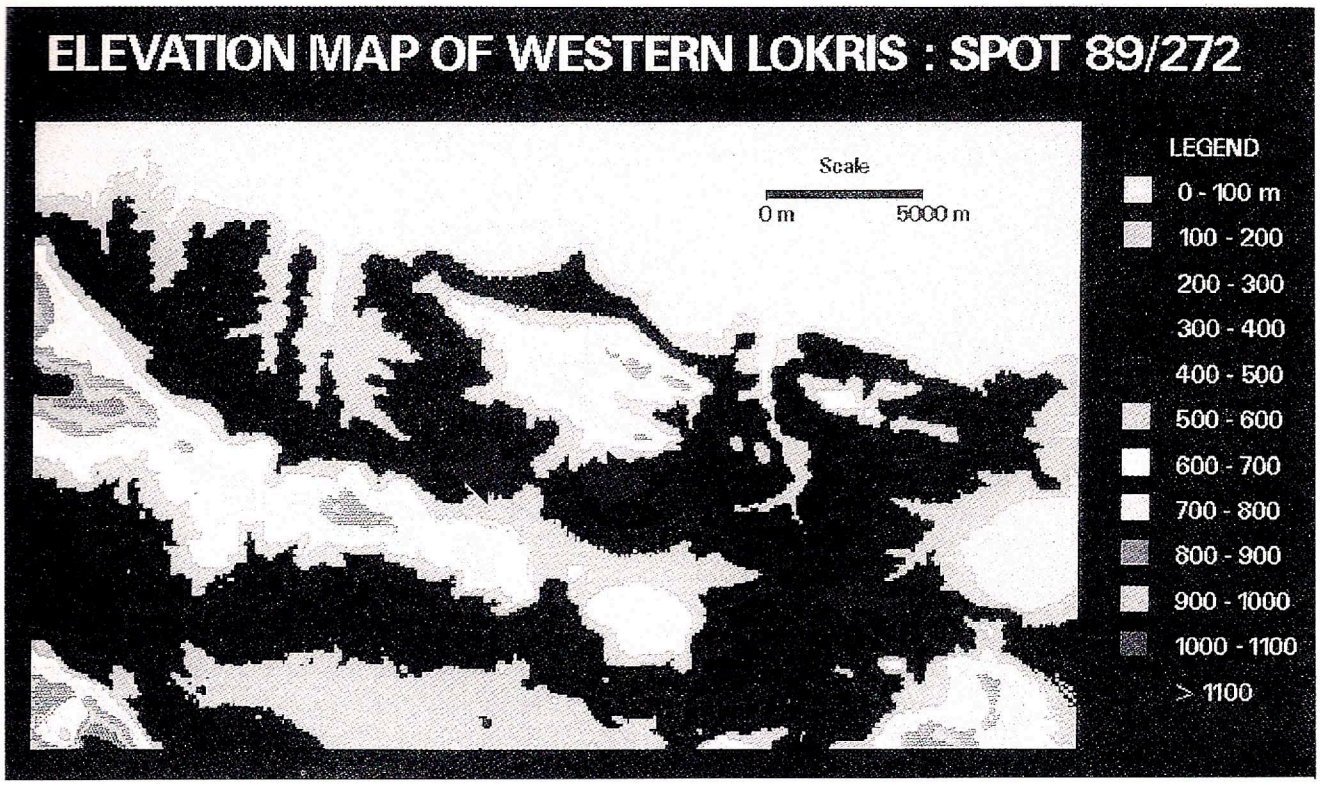

See plate I at end of volume

Figure 3. Image showing a thematic elevation map of the Western Lokris area, Central Greece (22.500 E to 23.000 E and 38.500 N to 38.800 N). The map was produced in ARC-GRID after importing the DEM intensity image from ERDAS Imagine. Elevations are grouped into twelve classes, each one shown with a different colour (see legend).

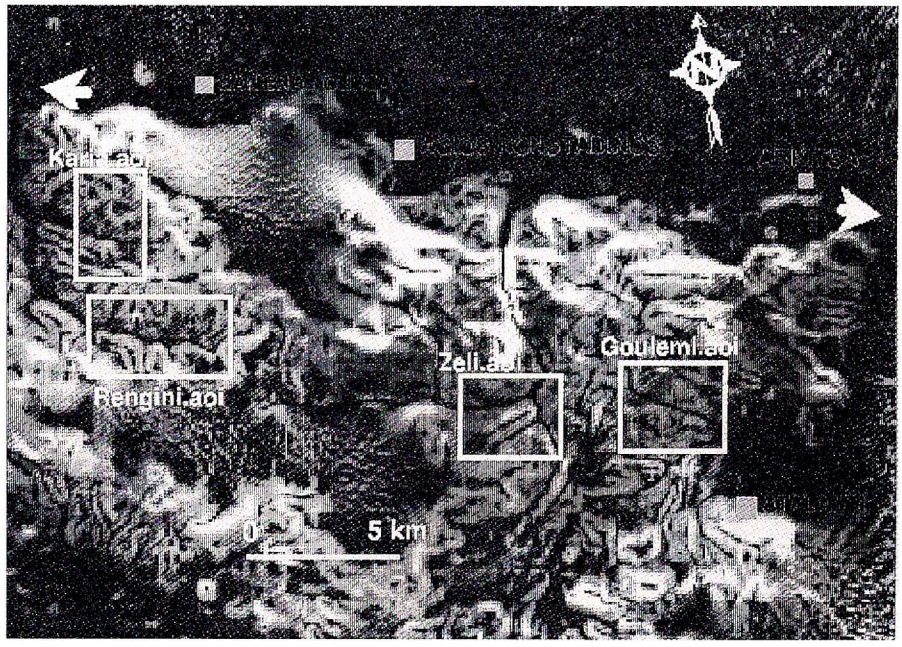

See plate I at end of volume

Figure 4. a) Image showing slope angle calculations for the region in Figure 3 (Western Lokris, Central Greece). The image is in raster format and its intensity varies proportionally with slope angle , that is bright areas correspond to high slopes. Also shown are four rectangular areas at the footwall of the Kammena Vourla Fault Segment, selected for statistical analysis. Text refers to population centres of the area. Notice the "grainy" texture at high elevations (compare with figure 3), resulted from the poor quality DEM data at these regions. b). The frequency distribution of slope angles at four areas in the footwall of the Kammena Vourla Fault Segment. Vertical axes numbers represent frequency of slope angle occurrence within each of the footwall area.

where Δ_{EW} and Δ_{NS} are the sums of elevation differences of the neighbouring pixels in the x-direction (rows) and in the y-direction (columns; ERDAS Field Guide page 322; the slope angle is the inverse tangent of s multiplied by $180/\pi$). The resultant slope map (Figure 4a) suffers from degraded resolution in the badly stereomatched areas expressed as an abrupt loss on geomorphic consistency (i.e. unconnected ridges and channels) in those areas. Over most of the Kammena Vourla hinterland, however, the map is consistent and four rectangular areas were extracted as areas of interest (AOIs, see boxes in Figure 4a) to obtain footwall statistics. The AOIs are located to the south of the dome-shaped coastal fault (Kammena Vourla) seen in Figure 2a and to the north of the second segment (Kallidromon) away from the rift axis. The size (ci. 3 × 3 km) and spacing (≥ 1 km) of these footwall areas are large enough to avoid any sampling bias. There are two important observations in these graphs (Figure 4b): first, all histograms are unimodal and second, mean values cluster around 8 degrees. This dual similarity in the distributions reflects a spatial dependence of slopes over distances at least as large as the distance from the Karia.aoi to Goulemi.aoi (Figure 4a). We suggest this is due to similar footwall uplift rates from the area south of Kammena Vourla (west) up to the area south of the town of Arkitsa (east; Figure 4a). No other material or topological property varies within this wavelength : erosion rates may be assumed the same for all areas because underlying lithology is mostly syn-rift (see key in Figure 1) and mean elevations of these areas range between 200 and 400 m (Figure 3; HAGS, 1977). These quantitative data (Figure 4) record a finite deformation of the footwall area and strongly indicate that the size of the Kammena Vourla fault segment is comparable to the longitudinal distance of the sampling areas, that is between 30-35 km.

CONCLUSIONS

This paper uses a DEM in order to analyse topographic data, drainage patterns and footwall slope statistics and to assess their implications for fault segmentation models. The results of the morphometric analysis (Figures 3 and 4) in the Western Lokris region of Central Greece support a long (30-35 km) segment length model at least for two of the normal fault segments of the area, the Kammena Vourla and Kallidromon Fault Segments. The former is the most active of the two as the Kallidromon fault deviates from the dome-shape geometry towards its northern tip (Figure 2) and its hangingwall area has been deformed (Figure 3). Over the 30-35 km distance wavelength, the footwall slopes of the Kammena Vourla segment exhibit a statistical homogeneity (Figure 4b), and the elevation profile (Figure 2) along strike has a dome-shape appearance. This is achieved by a systematic variation in footwall uplift. As footwall uplift also varies across strike of fault segments, because of block tilting being greater closer to the fault plane (e.g., Stein *et al.*, 1988), a 3D ellipsoidal configuration may be expected to form in the hinterland of isolated fault segments. This configuration may be seen in Figure 2a where an oblique perspective view is shown.

It is suggested that the DEM methodology presented here can be also applied to other continental rift systems to supply independent evidence in fault segment mapping. The objective would be to recognise two characteristic properties of isolated fault segments : i) dome-shaped strike-profiles and ii) ellipsoidal configurations of footwall volumes over distances of 30-35 km.

The information obtained from the DEM analysis can be further used in characterising the seismogenic potential of active faults by calculating maximum earthquake magnitudes expected in future events, from empirical seismological relationships such as rupture length vs magnitude (e.g. Wells and Coppersmith, 1994). The seismogenic potential is a useful parameter in hazard studies (e.g. dePolo and Slemmons, 1990). For instance, if we assume that the maximum surface rupture length (SRL) along an active normal fault segment equals the length of the segment then the size (M) of the associated earthquake can be estimated by the formula (Wells and Coppersmith, 1994):

$$M = 4.86 + 1.32 LogSRL, (\sigma = 0.34)$$

For the Kammena Vourla-Arkitsa segment (Figure 1), SRL=36 km, so M_{max}=6.9. Simirarly, for the Kallidromon Segment (38 km), M_{max}=6.9, as well. These estimates are in broad agreement with past historical events in the area (Papazachos and Papazachou, 1989).

Acknowledgements.

We are grateful to Prof. Peter Muller (UCL) for making available to us the software *3D-Image Maker* and the SPOT 1A imagery; Dr. Gerald Roberts (Birkbeck College, London) for many discussions on fault segmentation; Matt Roberts and Andy Banks for help with image processing and Dr. Kevin Hodges who provided UNIX support at various stages of the work. We also thank two anonymous referees. AG's research was funded by an IKY doctoral studentship and the University of Reading.

REFERENCES

Abbott, L. D., Silver, E. A., Anderson, R. S., Smith, R., Ingle, J. C., Kling, S. A., Haig, D., Small, E., Galewsky, J., and Sliter, W., 1997. Measurement of tectonic surface uplift rate in a young collisional mountain belt. Nature, 385, 501-507.

Ambraseys, N. N., and Jackson, J. A., 1990. Seismicity and associated strain of central Greece between 1890 and 1988. Geophys. J. Intern., 101, 663-708.

Anders, M. H., and Schlische, R. W., 1994. Overlapping faults, intrabasin highs, and the growth of normal faults. Journal of Geology, **102**, 165-180.

Bolstad, P. V., and Stowe, T., 1994. An evaluation of DEM accuracy : Elevation, Slope and Aspect. Photogr. Eng. & Rem. Sens., 60(11), 1327-1332.

Day, T., and Muller, J.-P., 1989. Digital elevation model production by stereo-matching spot image-pairs : a comparison of algorithms. Image and Vision Computing, 7, 95-101.

Deffontaines, B., Lee, J. -C., Angelier, J., Carvalho, J., and Rudant, J. -P., 1994. New geomorphic data on the active Taiwan orogen : a multisource approach. J. Geophys. Res., 99, 20243-20266.

dePolo, C. M., and Slemmons, D. B., 1990. Estimation of earthquake size for seismic hazards. In Krinitzsky, E. L., and Slemmons, D. B., Neotectonics in earthquake evaluation, Boulder, Colorado, Geol. Soc. America Reviews in Engineering Geology, 8, 1-28.

ERDAS Imagine ver 8.1 Field Guide. Third edition (July 1994), 628p.

Ganas, A., and White, K., 1996. Neotectonic fault segments and footwall geomorphology in Eastern Central Greece from Landsat TM data. Geol. Soc. Greece Sp. Publ., 6, 169-175.

Ganas, A., Wadge, G., and White, K., 1996. Fault Segmentation and Tectonic Geomorphology in Eastern Central Greece from Satellite Data. Eleventh ERIM Conference on Applied Geologic Remote Sensing Proceedings, Las Vegas 27-29 February 1996, **I**, 119-128.

Ganas, A., Roberts, G.P., and Memou, Tz., in press. Segment boundaries, the 1894 ruptures and strain patterns along the Atalanti Fault, central Greece. Journal of Geodynamics.

HAGS, 1977. 1: Stylis Map Sheet, 100 000 Map series. Athens.

Jones, C. H., Unruh, J. R., and Sonder, L. J., 1996. The role of gravitational potential energy in active deformation in the southwestern United States. Nature, 381, 37-41.

Massonnet, D., and Feigl, K. L., 1995. Satellite radar interferometric map of the coseismic deformation field of the M_w=6.1 Eureka Valley, California earthquake of May 17, 1993. Geophys. Res. Let., 22(12), 1541-1544.

Murphy, W., 1993. Remote sensing of active faults : case studies from southern Italy. Z. Geomorph. N. F., Suppl. -Bd. 94, 1-23.

Otto, G. P., and Chau, T .K. W., 1989. "Region-growing" algorithm for matching of terrain images. Image and Vision Computing, 7 (2), 83-94.

Papazachos, B., and Papazachou, K., 1989. The earthquakes of Greece. Ziti editions, Thessaloniki.

Roberts, G. P., and Koukouvelas, I., 1996. Structural and seismological segmentation of the Gulf of Corinth Fault System : implications for models of fault growth. Annali di Geophysica, XXXIX, 619-646.

Roberts, S., and Jackson, J., 1991. Active normal faulting in central Greece : an overview. In : Roberts, A. M., Yielding, G., and Freeman, B., (eds), The Geometry of Normal Faults. Geological Society Special Publication 56, 125-142.

Stein, R. S., King, G. C. P., and Rundle, J. B., 1988. The growth of geological structures by repeated earthquakes 2. Field examples of continental dip-slip faults. J. Geophys. Res., 93, 13319-13331.

Wells, D. L., and Coppersmith, K. J., 1994. New empirical relatiosnships among Magnitude, Rupture Length, Rupture Width, Rupture Area, and Surface Displacement. Bull. Seism. Soc. America, 84, 974-1002.